Chinese Chemical Letters 36 (2025) 110190

Contents lists available at ScienceDirect

Chinese Chemical Letters

journal homepage: www.elsevier.com/locate/cclet

The synthesis and evaluation of novel BPA derivatives for enhanced blood-brain barrier penetration and boron neutron capture therapy

Shushan Mo[a,b,1], Zhaoshuo Wang[c,1], Dandan Ding[a], Zhengzheng Yan[a], Yunlu Dai[d], Jinchao Zhang[e], Huifang Liu[b], Tianjiao Liang[f], Jianfei Tong[f], Zhenhua Li[a,*], Xueyi Wang[a,*]

[a] The Tenth Affiliated Hospital, Southern Medical University (Dongguan People's Hospital), Dongguan 523059, China
[b] College of Pharmaceutical Sciences, Key Laboratory of Pharmaceutical Quality Control of Hebei Province, Hebei University, Baoding 071002, China
[c] Growth Factors, Nutrients and Cancer Group, Spanish National Cancer Research Center (CNIO), Madrid 28029, Spain
[d] Cancer Centre and Institute of Translational Medicine, Faculty of Health Sciences, University of Macau, Macau SAR 999078, China
[e] College of Chemistry & Materials Science, Key Laboratory of Medicinal Chemistry and Molecular Diagnosis of Ministry of Education, State Key Laboratory of New Pharmaceutical Preparations and Excipients, Chemical Biology Key Laboratory of Hebei Province, Hebei University, Baoding 071002, China
[f] Spallation Neutron Source Science Center, Dongguan 523803, China

ARTICLE INFO

Article history:
Received 28 March 2024
Revised 25 June 2024
Accepted 27 June 2024
Available online 27 June 2024

Keywords:
Boron neutron capture therapy (BNCT)
Novel BPA derivatives
Boron drug development
BBB penetration
Glioblastoma

ABSTRACT

Boron neutron capture therapy (BNCT) has emerged as a promising treatment for cancers, offering a unique approach to selectively target tumor cells while sparing healthy tissues. Despite its clinical utility, the widespread use of fructose-BPA (F-BPA) has been hampered by its limited ability to penetrate the blood-brain barrier (BBB) and potential risks for patients with certain complications such as diabetes, hyperuricemia, and gout, particularly with substantial dosages. Herein, a series of novel BPA derivatives were synthesized. After the primary screening, geniposide-BPA (G-BPA) and salidroside-BPA (S-BPA) exhibited high water solubility, low cytotoxicity and safe profiles for intravenous injection. Furthermore, both G-BPA and S-BPA had demonstrated superior efficacy *in vitro* against the 4T1 cell line compared with F-BPA. Notably, S-BPA displayed optimal BBB penetration capability, as evidenced by *in vitro* BBB models and glioblastoma models *in vivo*, surpassing all other BPA derivative candidates. Meanwhile, G-BPA also exhibited enhanced performance relative to the clinical drug F-BPA. In brief, G-BPA and S-BPA, as novel BPA derivatives, demonstrated notable safety profiles and remarkable boron delivery capabilities, thereby offering promising therapeutic options for BNCT in the clinic.

Boron neutron capture therapy (BNCT) is an emerging and rapidly developing precision diagnosis and treatment technology in the field of tumor therapy, known as the "fifth therapy" after surgery, traditional radiotherapy, chemotherapy, and immunotherapy [1]. Recently, the integration of accelerator-based neutron sources within hospital settings has revolutionized treatment options, igniting a fresh wave of enthusiasm for the potential of BNCT in the world [2,3]. In the fundamental concept of BNCT, the interaction between neutrons and boron (^{10}B) facilitates a fission reaction, triggering the liberation of a recoiling ^{7}Li nucleus and α particle with high linear energy transfer. This event induces significant DNA damage, notably in the form of double-strand breaks. Attributed to the relatively short path lengths of these particles, approximately equivalent to the diameter of a cell, irradiation damage selectively targets cancer cells with ample boron content while sparing neighboring normal cells [4-7].

The most widely used boron agent in BNCT clinical trials is L-4-dihydroxyborylphenylalanine, commonly known as BPA [8,9]. As a boron-enriched derivative of the essential amino acid phenylalanine, BPA can be taken up into tumor cells by L-type amino acid transporter 1 (LAT1) [10-12]. However, the advancement of its clinical application faced challenges due to its poor water solubility attributed to the neutral charge at physiological pH and the hydrophobic nature of phenylalanine [13]. In response to this issue, Yoshino *et al.* innovatively synthesized a BPA derivative fructose-BPA (F-BPA) by forging covalent bonds between fructose and boronic acids in BPA, resulting in enhanced water solubility [14]. As a result, F-BPA has emerged as the preferred option in contemporary clinical investigations. Moreover, it is crucial to acknowledge the challenge of maintaining optimal concentration within cells during the BNCT process, attributed to the efflux of in-

* Corresponding authors.
E-mail addresses: zhenhuali@hbu.edu.cn (Z. Li), ixueyi@smu.edu.cn (X. Wang).
[1] These authors contributed equally to this work.

https://doi.org/10.1016/j.cclet.2024.110190
1001-8417/

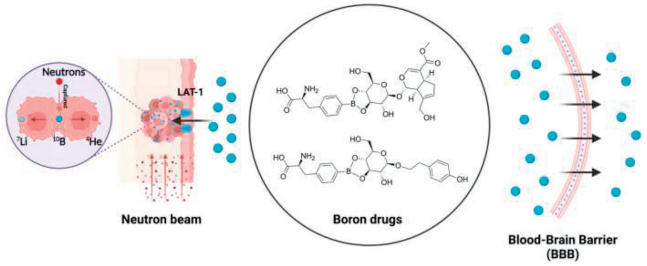

Fig. 1. Schematic illustration of G-BPA and S-BPA enhancing BNCT effect *in vitro* and boron uptake in glioblastoma *in vivo*. The figure was created with BioRender.com.

tracellular BPA *via* LAT1. Hence, in clinical practice, F-BPA is always administered to patients continuously both before and throughout the entire irradiation procedure to maintain high boron levels within tumors [15,16]. Consequently, a substantial quantity of fructose is introduced into the patients' bodies. However, large amounts of fructose may trigger severe adverse effects in certain patients dealing not only with cancer but also other ailments [17]. For instance, it can lead to insulin resistance in cancer patients with diabetes [18], as well as an uptick in uric acid levels in patients with hyperuricemia and gout [19,20]. Thus, the sharp elevation of fructose in the blood may bring a higher incidence of disease and worsen symptoms in complex cancer patients. Moreover, low delivery of F-BPA to glioblastoma was confirmed due to the blood-brain barrier (BBB) [21-24]. Hence, there arises an imperative need to seek out new small molecules as substitutes for fructose to bind with BPA, forming novel BPA derivatives for BNCT. This pursuit aims not only to enhance the water solubility of BPA and improve its accumulation in tumors, particularly in glioblastoma, but also to reduce the risk of additional complications for complex cancer patients undergoing BNCT treatment.

In our study, we selected several natural molecules containing diol group as substitutes for fructose, forming novel BPA derivatives, including geniposide, salidroside, levodopa, ascorbic acid, sialic acid, phlorizin, arbutin, aesculin, gastrodin, 5′-deoxy-5-fluorocytidine and 5-fluorocytidine. More importantly, most of these natural molecules were reported with certain ability to penetrate BBB, including salidroside [25], levodopa [26], ascorbic acid [27], sialic acid [28] and gastrodin [29]. Through meticulous screening based on water solubility and drug safety parameters, we identified geniposide-BPA (G-BPA) and salidroside-BPA (S-BPA) (Fig. 1) as the primary candidates, demonstrating excellent water solubility while maintaining drug safety profiles. Notably, they exhibited superior performance over F-BPA in terms of ^{10}B uptake and the BNCT effect within the 4T1 cell line. Moreover, these compounds showed enhanced efficiency in boron delivery across BBB models *in vitro* and glioblastoma models *in vivo*. These findings emphasized the potential of G-BPA and S-BPA, particularly the latter, in boron delivery across BBB or BNCT treatments, offering a promising BNCT drug option for tumor patients with multiple complex diseases.

In the pursuit of creating novel BPA derivatives, geniposide, salidroside, levodopa, ascorbic acid, sialic acid, phlorizin, arbutin, aesculin, gastrodin, 5′-deoxy-5-fluorocytidine, and 5-fluorocytidine were chosen as substitutes for fructose to bind with BPA through boron ester bonds (Figs. S1 and S2 in Supporting information). During the preparation process, the hydrochloride salt of BPA (BPA·HCl) was synthesized to address BPA's poor solubility in both water and organic solvents. BPA·HCl was then reacted with various diol-containing natural molecules in a DMSO solvent. Post-reaction, excess BPA was removed through repeated filtration in water. Finally, the pure BPA derivatives were obtained after freeze-

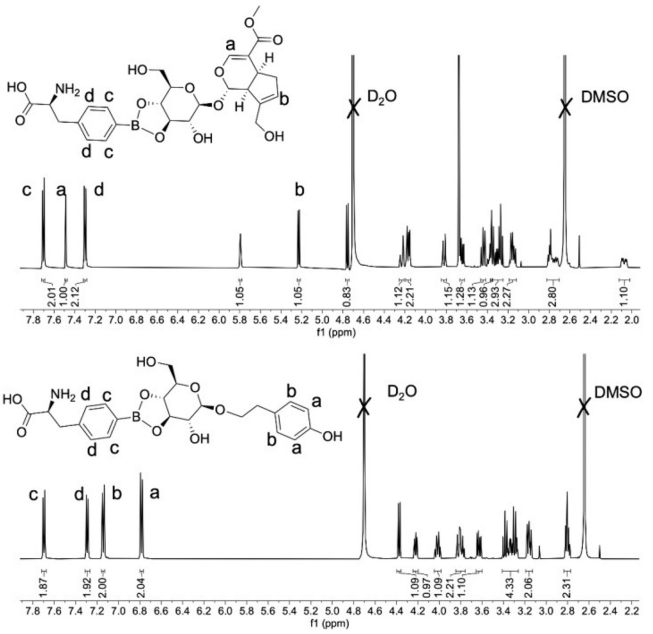

Fig. 2. ^{1}H NMR (D_2O) spectrum of G-BPA and S-BPA. The corresponding protons are marked in the structures.

drying. This provided an easy and efficient synthesis method to prepare novel BPA derivatives as potential drugs for BNCT. The synthesis efficiencies of all the novel BPA derivatives were above 84%. This BPA-based synthesis method is not only extremely simple and suitable for large-scale production but also addresses the problem of insufficient sources of ^{10}B drugs. These compounds formed the basis of potential breakthroughs in boron drug development. The structure and corresponding ^{1}H nuclear magnetic resonance (NMR) results of G-BPA and S-BPA were shown in Fig. 2, and the others were shown in Figs. S3–S11 (Supporting information). Based on all the ^{1}H NMR results, the integral ratios between the characteristic peaks in novel BPA derivatives matched the theoretical values precisely. Furthermore, in comparison to BPA (Fig. S12 in Supporting information), the hydrogen peaks on the benzene ring of the newly synthesized BPA derivatives exhibited significant chemical shifts. Besides, the successful synthesis of G-BPA and S-BPA was also confirmed by electrospray ionization tandem mass spectrometry (ESI-MS) (Figs. S13 and S14 in Supporting information). As a result, all the novel BPA derivatives significantly improved the solubility of BPA, and they could keep stable in phosphate buffered saline (PBS) buffer solution at pH 7.4. It is worth noting that after the conjugation with the diol-containing natural molecules, the formed BPA derivatives turned sticky liquid from the colorless powder of BPA.

Subsequently, the initial pool of candidates underwent rigorous assessment, primarily focusing on water solubility. Given the necessity of high boron concentration in tumor tissues for BNCT, the selected boron drugs needed to exhibit super water solubility, reaching levels as high as 4790 ppm ^{10}B. Notably, phlorizin-BPA and aesculin-BPA were excluded from contention due to the formation of aggregates. The remaining candidates underwent further screening concerning drug safety, involving the injection at a dosage of 598 μg ^{10}B per mouse *via* tail vein injection. As a result, after the injection, only the mice in G-BPA and S-BPA groups all survived (Table S1 in Supporting information). Thus, within the realm of novel BPA derivatives, only G-BPA and S-BPA demonstrated promising prospects for BNCT applications, particularly in terms of drug safety.

In order to further validate the safety profile of the drug and assess the cytotoxic effects of G-BPA and S-BPA, two distinct cell

lines, 4T1 and U87 MG, were chosen for comprehensive evaluation. Specifically, a range of concentrations (ranging from 0.032 ppm to 20 ppm ^{10}B) of F-BPA (control group), G-BPA, and S-BPA were individually introduced to the cells. As a result, Fig. S15 (Supporting information) illustrated that G-BPA (Fig. S15b) and S-BPA (Fig. S15c), similar to F-BPA (Fig. S15a), exhibited negligible impact on 4T1 viability, even at concentrations as high as 20 ppm. Similarly, the effects of F-BPA (Fig. S15d), G-BPA (Fig. S15e), and S-BPA (Fig. S15f) on the viability of U87 MG cells were also investigated. Consistent with the findings for 4T1 cells, G-BPA and S-BPA demonstrated minimal proliferation inhibition on U87 MG at concentrations below 20 ppm, mirroring the behavior of F-BPA. Hence the results of cytotoxicity studies further demonstrated the safety profile of G-BPA and S-BPA, highlighting their promising prospects for utilization in BNCT.

Serum chemistry and hematological analysis are essential indicators of drug biosafety *in vivo*, providing insights into the body's physiological and biochemical state. Thus, we meticulously evaluated these parameters to ensure a comprehensive biosafety assessment. On day 3 post-intravenous injection with G-BPA, S-BPA, F-BPA, and PBS (control group), the detailed serum chemistry and blood indices analysis were conducted. As presented in Tables S2 and S3 (Supporting information), the results indicated no significant alterations in hepatic function, kidney function, myocardial enzyme levels, or blood indices across the G-BPA, S-BPA, F-BPA, and control groups. All measured values remained within the normal physiological range, indicating stable organ function and the absence of systemic toxicity. These findings demonstrated that G-BPA and S-BPA do not induce significant systemic toxicity.

Besides, the boron delivery ability of novel BPA derivatives was investigated, as a crucial factor in advancing delivery agents for BNCT. As illustrated in Fig. 3a, the intracellular uptake of ^{10}B by cultured 4T1 cells incubated with G-BPA and S-BPA for 3 h, significantly surpassed that observed with F-BPA. This trend was evident across varying ^{10}B concentrations of 5, 10, and 20 ppm. For example, at ^{10}B concentrations of 20 ppm, the uptake of F-BPA was about 123 ng per 10^6 cells. In contrast, the uptake of G-BPA and S-BPA exhibited enhancements, reaching near 180 and 186 ng per 10^6 cells, respectively. These results indicated that geniposide and salidroside as the solubilizer could significantly improve the boron delivery ability of BPA, compared with fructose. Consequently, G-BPA and S-BPA emerged as superior choices over F-BPA for efficiently delivering sufficient ^{10}B to 4T1 cells.

Notably, the intracellular uptake of BPA, F-BPA has been reported to occur *via* LAT1 [10,11]. Thus, the mechanism of intracellular uptake of G-BPA and S-BPA was also investigated. This was performed both with and without the LAT1 inhibitor 2-amino-2-norbornanecarboxylic acid (BCH). As illustrated in Fig. S16 (Supporting information), when BCH was introduced, there was a significant reduction in the cellular uptake of both F-BPA, G-BPA and S-BPA in 4T1 cell line. Moreover, the BCH inhibition efficiencies were very similar (F-BPA: 46.3%, G-BPA: 43.9%, S-BPA: 45.2%). This decrease indicated that G-BPA and S-BPA were indeed recognized by LAT1. These findings were particularly noteworthy as they confirmed that G-BPA and S-BPA may be internalized into cells *via* LAT1-mediated transport, like F-BPA. Moreover, the intracellular uptake of BPA in NIH 3T3 cell lines with and without BCH was also conducted and quantified. As shown in Fig. S17 (Supporting information), the addition of BCH reduced the uptake of F-BPA, G-BPA and S-BPA slightly in NIH 3T3 cell line, indicating the low expression of LAT1 in normal cells compared with tumor cells. Moreover, the uptake of ^{10}B in NIH 3T3 cells was significantly lower than the uptake in 4T1 cells (Fig. S18 in Supporting information), further demonstrating the low expression of LAT1 in normal cells and LAT1 dependent uptake of F-BPA, G-BPA and S-BPA.

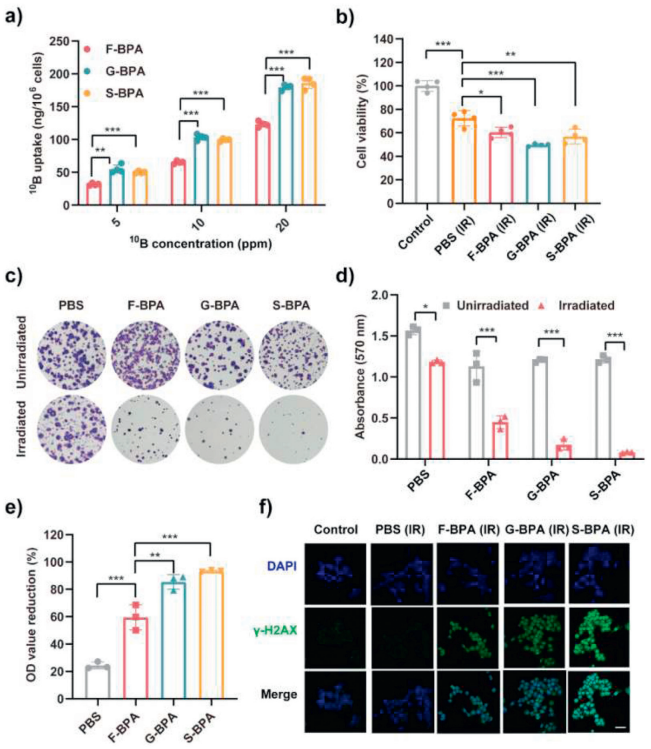

Fig. 3. The BNCT effect evaluation of F-BPA, G-BPA, and S-BPA *in vitro* in 4T1 cell line. (a) Cellular ^{10}B uptake by 4T1 cells at different ^{10}B concentrations for 3 h (n = 4). (b) The killing effect of neutron radiation on 4T1 cells in F-BPA, G-BPA, and S-BPA groups, measured by CCK-8 assay (n = 4). (c) Cell colony formation after neutron radiation treatment in F-BPA, G-BPA and S-BPA groups and colonies were stained with crystal violet. (d) Absorbance of crystal violet solution dissolved in 10% acetic acid from colonies in F-BPA, G-BPA and S-BPA groups, recording the OD values at 570 nm (n = 3). (e) The OD value reduction of crystal violet solution dissolved from cell colonies, compared the samples before and after neutron radiation treatment (n = 3). (f) Representative immunofluorescence images were recorded using CLSM. Nuclei were stained with 4′,6-diamidino-2-phenylindole (DAPI, blue) and the γ-H2AX was visualized *via* antibody labeling (green). IR means "irradiated". Scale bar: 50 μm. Data are presented as the mean ± standard deviation (SD) of measurements. $^*P < 0.05$, $^{**}P < 0.01$, $^{***}P < 0.001$.

Furthermore, to further evaluate the BNCT effect in breast cancer *in vitro* for G-BPA and S-BPA, cell counting kit-8 (CCK-8) assay, cell colony assay and DNA double-strand breaks test were carried out after the neutron irradiation, separately.

To explore the immediate impact of neutron irradiation on the viability of ^{10}B-containing cells, 4T1 cells were co-incubated with F-BPA, G-BPA and S-BPA at ^{10}B concentrations of 5 ppm for 3 h before neutron exposure. Following irradiation, the immediate cytotoxic effects on 4T1 cells were assessed using CCK-8 after 18 h. Notably, compared with the control samples without neutron irradiation, a minor fraction of cells were directly killed by irradiation (Fig. 3b). Furthermore, after neutron irradiation, 4T1 cells in the F-BPA group exhibited viability of 60.4%. While the viabilities of G-BPA and S-BPA groups maintained 49.7% and 56.9%, respectively. Consequently, when comparing F-BPA, G-BPA, and S-BPA at identical ^{10}B concentrations, a greater reduction in cell viability was observed in S-BPA and G-BPA groups after neutron irradiation *in vitro*. Moreover, this result was consistent with the boron uptake findings, confirming the association between BNCT efficacy and intracellular ^{10}B concentrations.

Previous research has illuminated the potential of BNCT to induce DNA damage, posing challenges to DNA repair mechanisms and impeding cellular proliferation [4,15]. To investigate the efficiency of BNCT in different BPA derivative groups, the proliferation of post-irradiation 4T1 cells was evaluated using a cell colony

assay, assessing the individual cells' capacity to form and expand colonies. After neutron irradiation, 4T1 cells in different groups were given five days to thrive before being treated with a crystal violet stain. In Fig. 3c, it is evident that the colonies observed in the F-BPA, G-BPA, and S-BPA groups were significantly fewer compared with those in the control groups, indicating the BNCT effect in hindering cell proliferation. As shown in Fig. S19 (Supporting information), by analyzing colonies containing over 50 cells, the colony count decreased from 368 to 40.7 by a reduction of 88.8% in the S-BPA group following irradiation, in contrast to the unirradiated group. Similarly, for G-BPA and F-BPA, the respective reduction percentages were 75.9% and 55.5%. Furthermore, the optical density (OD) values of the crystal violet solution in each group were assessed using a microplate reader to assess cellular activity. Illustrated in Figs. 3d and e, the OD value of the S-BPA group post-irradiation was the lowest at 0.08, with the highest reduction percentage of 93.4% observed in this group, in accordance with the colony count results. Besides, the reduction percentages in G-BPA and F-BPA groups were 85.5% and 59.5%, respectively. Thus, these results conclusively validated that the integration of BNCT with S-BPA or G-BPA, particularly the former, exhibited excellent efficacy in impeding the proliferation of 4T1 cells, surpassing that of F-BPA. Besides, the same cell colony assay was also performed in the NIH 3T3 cell line to evaluate the cell proliferation ability post-irradiation. On the contrary, the BNCT efficiency was low in all experiment groups in NIH 3T3 cell line (Fig. S20 in Supporting information), confirming the significant positive relationship between ^{10}B uptake and BNCT efficiency *in vitro*.

Besides, to validate the occurrence of DNA double-strand breaks induced by BNCT *in vitro*, immunofluorescence analysis of phosphorylated histone H2AX (γ-H2AX) staining on 4T1 cells incubated with different BPA derivatives was conducted. As illustrated in Fig. 3f, an obvious display of green fluorescence within the nucleus was observed in the F-BPA, G-BPA, and S-BPA groups compared with control groups devoid of neutron irradiation or boron drugs. This compelling observation indicated that BNCT was a powerful therapy to induce substantial DNA double-strand breaks *in vitro*, consistent with previous reports [4-7]. Notably, the intensity of green fluorescence within the nucleus was significantly higher in the S-BPA group compared with the F-BPA and G-BPA groups, suggesting S-BPA could greatly enhance the formation of DNA double-strand breaks with BNCT in breast cancer *in vitro*. Moreover, these results were also confirmed by the fluorescence qualification of the γ-H2AX foci by confocal laser scanning microscopy (CLSM) (Fig. S21 in Supporting information).

In the subsequent phase to assess their capacity to penetrate the BBB, G-BPA and S-BPA underwent comprehensive testing in U87 MG cell line, including *in vitro* BBB models, and glioblastoma models *in vivo*. All animal experiments were approved by the Dongguan People's Hospital Ethics Committee and conducted following the Regulations for the Administration of Affairs Concerning Experimental Animals (P. R. China). This assessment held significant importance for glioblastoma patients, as the presence of the BBB consistently hampers drug delivery to the brain, leading to poor drug treatment. Thus, evaluating the BBB penetration ability of G-BPA and S-BPA was deemed crucial for their potential application in glioblastoma BNCT.

Initially, the cellular uptake of various BPA derivatives was conducted in U87 MG cells. Consistent with our findings in 4T1 cells, higher concentrations of ^{10}B were observed in U87 MG cells treated with G-BPA and S-BPA, across varying concentrations of 5, 10, and 20 ppm (Fig. 4a). This indicated a superior boron delivery capability of G-BPA and S-BPA to U87 MG cells compared with F-BPA.

Moreover, the cell colony assay was also performed in the U87 MG cell line to evaluate the cell proliferation ability post-

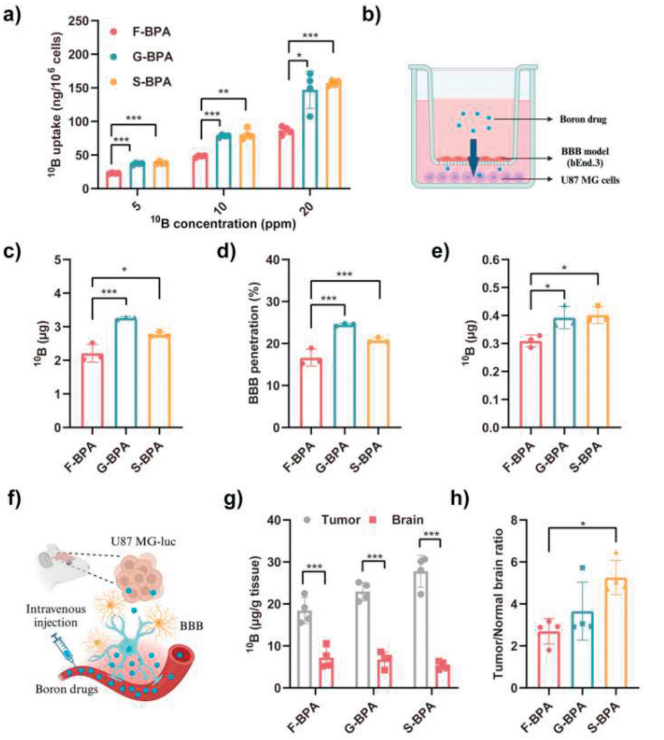

Fig. 4. The evaluation of F-BPA, G-BPA, and S-BPA in U87 MG cell line, BBB models *in vitro* and orthotopic glioblastoma mouse models *in vivo*. (a) Cellular ^{10}B uptake by U87 MG cells at different ^{10}B concentrations for 3 h (n = 4). (b) Schematic illustration of the boron drug evaluation in BBB models *in vitro*. (c) The ^{10}B content of F-BPA, G-BPA, and S-BPA which crossed the BBB *in vitro* from the insert to the chamber base (n = 3). (d) Percentages of F-BPA, G-BPA, and S-BPA which crossed the BBB *in vitro* (n = 3). (e) The uptake of ^{10}B in U87 MG cells in the chamber base after the BBB penetration of F-BPA, G-BPA, and S-BPA (n = 3). (f) Schematic illustration of boron drug evaluation in the orthotopic glioblastoma mouse models. (g) The content of ^{10}B distribution in tumor and normal brain after administrating F-BPA, G-BPA, and S-BPA (n = 4). (h) Tumor/normal brain ratio of ^{10}B in U87 MG-luc bearing nude mice after injecting F-BPA, G-BPA, and S-BPA respectively (n = 4). Data are presented as the mean ± SD of measurements. $^*P < 0.05$, $^{**}P < 0.01$, $^{***}P < 0.001$.

irradiation. As shown in Fig. S22 (Supporting information), similar to the cell colony assay results in 4T1 cells, the cell proliferation inhibition was also significant in G-BPA and S-BPA groups, and the cell proliferation inhibition efficiency was higher than 80% both in G-BPA and S-BPA groups, indicating the high efficiency of BNCT *in vitro* for G-BPA and S-BPA in U87 MG cell line.

The penetration ability of BPA derivatives across the BBB was evaluated using a transwell system as an *in vitro* BBB model as illustrated in Fig. 4b [30,31]. Then G-BPA, S-BPA, and F-BPA, each at a concentration of 13.3 μg ^{10}B, were introduced into the transwell insert, while U87 MG cells were cultured at the base of the transwell chamber. This facilitated the assessment of the penetration of BPA derivatives through the bEnd.3 cell layer and their uptake by U87 MG cells. As shown in Fig. 4c, the quantities of ^{10}B transported across the BBB model by G-BPA and S-BPA were notably higher, at 3.26 and 2.77 μg respectively, compared with 2.21 μg for F-BPA. In other words, 24.5% of G-BPA successfully penetrated the BBB model, while for S-BPA and F-BPA, the penetration efficiencies were 20.8% and 16.6% respectively (Fig. 4d). Moreover, the uptake of ^{10}B by U87 MG cells at the base of the transwell chamber varied across the different BPA derivative groups. Remarkably, as illustrated in Fig. 4e, the uptake of G-BPA and S-BPA exceeded that of F-BPA, owing to their superior penetration efficiency and enhanced cellular uptake capacity. Consequently, these experiments with the BBB model *in vitro* demonstrated the superior ability of G-BPA and

S-BPA to penetrate the BBB, thus indicating their greater therapeutic potential in glioblastoma BNCT.

For successful BNCT, one crucial factor was sufficient concentrations of ^{10}B accumulated in tumor (>20 μg ^{10}B per gram of tumor tissue) and a high tumor-to-normal tissue (T/N) ratio. Thus, G-BPA and S-BPA were continuously evaluated in glioblastoma models *in vivo*. The orthotopic glioblastoma mouse models were established and monitored by bioluminescence imaging [32]. Remarkably high bioluminescence intensity was detected within the brain, signifying robust proliferative activity of U87MG-luc cells (Fig. S23 in Supporting information). Subsequently, as shown in Fig. 4f, diverse BPA derivatives were intravenously administered to BALB/c nude mice bearing U87 MG-luc orthotopic glioblastoma, individually. At 1, 3, and 5 h post-injection, tissues from the heart, liver, spleen, lung, kidney, brain, tumor, and blood were collected and quantified using ICP-MS. As illustrated in Fig. S24 (Supporting information), the ^{10}B levels in tumor tissues were elevated in both S-BPA and G-BPA groups compared with F-BPA group, at 1 and 3 h post-injection. Specially, as shown in Fig. 4g, the ^{10}B content in G-BPA and S-BPA groups at 3 h surpassed the critical value 20 μg ^{10}B per gram of tumor tissue, highlighting a significant improvement in ^{10}B accumulation. In contrast, the ^{10}B content in F-BPA group at 3 h was lower than 20 μg ^{10}B per gram of tumor tissue. Moreover, the ^{10}B content of the normal brain in S-BPA, G-BPA, and F-BPA groups were notably lower than the ^{10}B uptake in the tumor from 1 h to 5 h (Fig. 4g and Fig. S25 in Supporting information). Besides, the ^{10}B uptake in other normal tissues and blood were measured and the results were shown in Figs. S26 and S29 (Supporting information). Thus, the T/N and T/B ratios in different BPA derivative groups were also analyzed. As a result, T/Brain ratios of S-BPA, G-BPA, and F-BPA groups at different hours were calculated and shown in Fig. 4h and Fig. S27 (Supporting information). At 3 h post-injection, the ^{10}B concentration ratios in the different BPA derivative groups reached their peak. The values in the G-BPA and S-BPA groups were notably higher than those in the F-BPA group. Specifically, at this time point, the ratio between glioblastoma and normal brain tissue in the S-BPA group was 5.26, nearly double the ratio observed in the F-BPA group, which was 2.69. Additionally, the T/B ratios for the S-BPA, G-BPA, and F-BPA groups were analyzed at various time points, as illustrated in Fig. S28 (Supporting information). The T/B ratios for the different BPA derivatives reached their peak at 3 h post-injection. Notably, the values for the G-BPA (3.89) and S-BPA (3.81) groups were significantly higher than those for the F-BPA (2.79) group. Furthermore, Fig. S29 (Supporting information) illustrated the analysis of T/N ratios at various time points. In detail, similar to T/Brain ratios, the other T/N ratios in different BPA derivative groups peaked at 3 h post-injection. Among all the T/N ratios, the T/K ratios were the lowest due to the main metabolism of BPA derivatives by the kidneys. It is noteworthy to highlight that while the enhancement in T/B and T/Brain ratios was evident, the improvement in other T/N ratios within the G-BPA and S-BPA groups was less pronounced at 1 and 5 h post-injection. However, a significant shift occurred at the 3 h mark, wherein both G-BPA and S-BPA demonstrated a remarkable capacity to enhance the T/N ratios, as illustrated in Fig. S29d. Consequently, both G-BPA and S-BPA not only facilitated increased ^{10}B accumulation in glioblastoma but also significantly improved the T/N ratio, indicative of their potential therapeutic efficacy. Particularly noteworthy was the superior uptake and distribution efficacy exhibited by S-BPA in glioblastoma models, underscoring its promising role in BNCT.

In summary, we synthesized a series of novel BPA derivatives, utilizing the binding affinity between BPA and the diol group of specific natural molecules. The primary objective was to enhance both the solubility and boron delivery efficacy of BPA. Subsequently, novel BPA derivatives were screened by water solubility and drug safety in mouse models. Remarkably, only G-BPA and S-BPA exhibited exceptional performance. Next, the biosafety profile of BPA derivatives was further confirmed by the cytotoxic effects in 4T1 and U87 MG cell lines, serum chemistry and hematological analysis. Besides, the enhancement of BNCT efficiency was confirmed for G-BPA and S-BPA in 4T1 cells, *via* CCK-8 assay, cell colony assay and DNA double-strand breaks detection after neutron irradiation. Furthermore, the penetration capacity of G-BPA and S-BPA across the BBB was assessed in U87 MG cell lines, including *in vitro* BBB models and glioblastoma models *in vivo*. Notably, S-BPA emerged as the optimal boron drug among all BPA derivatives discussed in this study, while G-BPA also exhibited superior performance compared with the clinical drug F-BPA. Consequently, G-BPA and S-BPA, as newly synthesized BPA derivatives, demonstrated notable safety profiles and remarkable boron delivery capability, notably excelling in the BBB penetration, thus presenting promising therapeutic avenues for BNCT treatment with enhanced efficiency.

Declaration of competing interest

The authors declare that they have no known competing financial interests or personal relationships that could have appeared to influence the work reported in this paper.

CRediT authorship contribution statement

Shushan Mo: Writing – original draft, Investigation, Data curation. **Zhaoshuo Wang:** Investigation, Data curation. **Dandan Ding:** Formal analysis. **Zhengzheng Yan:** Formal analysis. **Yunlu Dai:** Formal analysis. **Jinchao Zhang:** Methodology, Formal analysis. **Huifang Liu:** Methodology, Formal analysis. **Tianjiao Liang:** Formal analysis. **Jianfei Tong:** Formal analysis. **Zhenhua Li:** Writing – review & editing, Validation, Supervision, Resources, Project administration, Funding acquisition, Conceptualization. **Xueyi Wang:** Writing – review & editing, Writing – original draft, Supervision, Investigation, Data curation, Conceptualization.

Acknowledgments

This work was supported by Guangdong Basic and Applied Basic Research Foundation (No. 2021B1515120065), National Natural Science Foundation of China (Nos. 82202339, 32271420, 82202307), China Postdoctoral Science Foundation (Nos. 2022M711527, 2021M701640), Science Fund for Creative Research Groups of Nature Science Foundation of Hebei Province (No. B2021201038), National High-End Foreign Expert Recruitment Plan (No. G2022003007L), Natural Science Foundation of Hebei Province (No. B2023201108).

Supplementary materials

Supplementary material associated with this article can be found, in the online version, at doi:10.1016/j.cclet.2024.110190.

References

[1] R.F. Barth, A.H. Soloway, J. Neuro-Oncol. 33 (1997) 3–7.
[2] H. Igaki, N. Murakami, S. Nakamura, et al., Clin. Transl. Radiat. Oncol. 33 (2022) 128–133.
[3] M. Suzuki, Int. J. Clin. Oncol. 25 (2020) 43–50.
[4] J. Li, Q. Sun, C. Lu, et al., Nat. Commun. 13 (2022) 2143.
[5] L. Dai, J. Liu, X. Zhao, et al., Adv. Funct. Mater. 33 (2023) 2214145.
[6] Y. Shi, Z. Guo, Q. Fu, et al., Nat. Commun. 14 (2023) 1884.
[7] K. Chen, S. Liu, L. Lv, et al., Nano Today 52 (2023) 101995.
[8] M. Lamba, A. Goswami, A. Bandyopadhyay, Chem. Commun. 57 (2021) 827–839.
[9] A. Raitano, T. Martin, C. Zhang, et al., J. Med. Chem. 66 (2023) 13809–13820.
[10] T. Nomoto, Y. Inoue, Y. Yao, et al., Sci. Adv. 6 (2020) eaaz1722.

[11] T. Nomoto, Y. Yao, Y. Inoue, et al., J. Control. Release 332 (2021) 184–193.
[12] L. Li, B. Sun, J. Sun, L. Chen, Zh. He, Chin. Chem. Lett. 35 (2024) 109538.
[13] J. Matović, K. Bahrami, P. Stockmann, et al., Mol. Pharmaceutics 20 (2023) 3127–3139.
[14] Y. Mori, A. Suzuki, K. Yoshino, H. Kakihana, Pigm. Cell Res. 2 (1989) 273–277.
[15] J. Li, X. Wang, Z. Wang, et al., Biomater. Sci. 11 (2023) 7568–7578.
[16] Q. Dai, Q. Yang, X. Bao, et al., Mol. Pharmaceutics 19 (2022) 363–377.
[17] W.C. Dornas, W.G. de Lima, M.L. Pedrosa, M.E. Silva, Adv. Nutr. 6 (2015) 729–737.
[18] K. Tornheim, J.M. Lowenstein, J. Biol. Chem. 251 (1976) 7322–7328.
[19] J. Jeppesen, Y.I. Chen, M.Y. Zhou, et al., Am. J. Clin. Nutr. 61 (1995) 787–791.
[20] D.D. Wang, J.L. Sievenpiper, R.J. de Souza, et al., J. Nutr. 142 (2012) 916–923.
[21] J. Stalinska, C. Vittori, C.H. Ingraham Iv, et al., Sci. Rep. 12 (2022) 3384.
[22] C.H. Ingraham, J. Stalinska, S.C. Carson, et al., Sci. Rep. 13 (2023) 12236.
[23] N. Kuthala, R. Vankayala, Y.N. Li, et al., Adv. Mater. 29 (2017) 1700850.
[24] M. Li, W. Zhang, J. Li, et al., Chin. Chem. Lett. 34 (2023) 108177.
[25] R. Vengoji, M.A. Macha, S.K. Batra, N.A. Shonka, Oncotarget 9 (2018) 22194–22219.
[26] L. Peura, K. Malmioja, K. Huttunen, et al., Pharm. Res. 30 (2013) 2523–2537.
[27] B. Xiong, Y. Wang, Y. Chen, et al., J. Med. Chem. 64 (2021) 13152–13173.
[28] B. Wang, J.A. Downing, P. Petocz, J.B. Miller, W.L. Bryden, Asia Pac. J. Clin. Nutr. 16 (2007) 110–115.
[29] Y. Mi, Y. Mao, H. Cheng, et al., Fitoterapia 140 (2020) 104447.
[30] I. Hubatsch, E.G.E. Ragnarsson, P. Artursson, Nat. Protoc. 2 (2007) 2111–2119.
[31] L. Shen, H. Liu, M. Jin, et al., Chin. Chem. Lett. 35 (2024) 109572.
[32] H. Wu, Y. Wang, Z. Ren, et al., Chin. Chem. Lett. 36 (2025) 109996.